ACS OMEGA

http://pubs.acs.org/journal/acsodf

Article

Numerical Simulation on Preparing Uniform and Stable Perovskite Wet Film in Slot-Die Coating Process

Qiang Guo, Xiaoli Gong, Zhenzhen Shen, Xia Hao,* and Jingquan Zhang

Cite This: *ACS Omega* 2023, 8, 19547−19555

Read Online

ACCESS | Metrics & More | Article Recommendations

ABSTRACT: Slot-die coating is regarded as a reliable and potential technology for preparing large-area perovskite solar cells with high efficiency and low cost. Therein, the formation of continuous and uniform wet film is of significance to obtain a high-quality solid perovskite film. In this work, the rheological properties of the perovskite precursor fluid are analyzed. Then, the ANSYS Fluent is introduced to establish an integrated model of internal and external flow fields during the coating process. The model is applicable to all perovskite precursor solutions with near-Newtonian fluids. Based on the theoretical simulation of finite element analysis, the preparation of 0.8 M-$FA_xCs_{1-x}PbI_3$, one of the typical large-area perovskite precursor solutions, is explored. Accordingly, this work indicates that the coupling process parameters like the fluid supply velocity (V_{in}) and coating velocity (V) determine the uniformity that the solution flows out of the slit and is coated onto the substrates, and the coating windows for a uniform and stable perovskite wet film is obtained. For the upper boundary range of the coating windows, the maximum value of V and V_{in} follows $V = 0.003 + 1.46V_{in}$ ($V_{in} \leq 0.1$ m/s), while for its lower boundary range, the minimum value of V and V_{in} is $V = 0.002 + 0.67V_{in}$ ($V_{in} \leq 0.1$ m/s). When V_{in} is higher than 0.1 m/s, the film will break due to the excessive V. Finally, the real experiment verifies the accuracy of the numerical simulation. Hopefully, this work is of reference value for the development of the slot-die coating forming process on the perovskite precursor solution approximating Newtonian fluid.

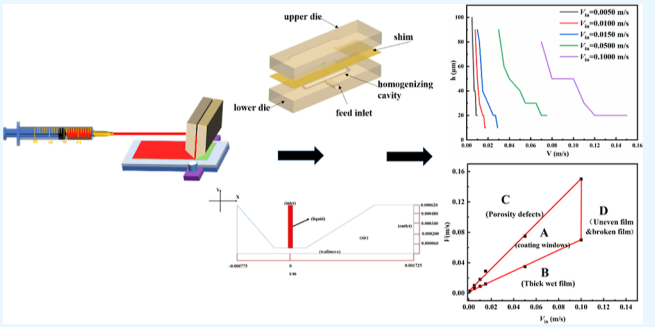

1. INTRODUCTION

The power conversion efficiency (PCE) of small-area polycrystalline perovskite solar cells (PSCs) has experienced a sharp increase from 3.8% in 2009 to 25.7% in 2022.[1−4] A variety of perovskite film deposition technologies are capable of making devices with a PCE of over 23%.[5−7] However, the PCE of modules with an area of >100 cm^2 is only 18.6% at present.[8] The substantial reduction of module efficiency after area amplification greatly limits the commercial promotion of PSCs. Therefore, how to realize the low-cost and large-area preparation of a perovskite film with high-quality polycrystalline is widely concerned in the photovoltaic field in recent years. Compared with vacuum deposition technologies like multisource co-evaporation,[9] the non-vacuum deposition technologies including spin-coating,[10] slot-die coating,[11] and blade coating[12] have the advantages of low equipment cost, simple process, and low expected manufacturing cost. Among them, the slot-die coating has been proved to have high repeatability, good film quality, and other characteristics, which are particularly suitable for preparing a large-area polycrystalline perovskite film.[13−15]

The main process of slot-die coating is that the precursor flowing from the slit of the coating head is uniformly coated on the substrate through the cutter head to obtain a liquid wet film.[16,17] The wet film can be converted into a solid polycrystalline perovskite film after post-treatment under certain conditions. By this way, the properties of the wet film directly determine the morphology of the subsequent perovskite film, which further affects the performance of PSCs.[11] The morphology of the wet film formed in the coating process is related to many parameters, such as die type, liquid supply velocity, coating velocity, solution fluid properties, and coating gap.[18−20] Therein, these parameters are coupled with each other to jointly affect the performance of devices, enhancing the complexity of adjusting and optimizing process parameters in actual experiments. Under this circumstance, the theoretical simulation is able to select and optimize key parameters in advance to a certain extent. As a result, the simulation of the slot-die coating process provides low-cost, simple, and direct theoretical support for the preparation of

Received: February 13, 2023
Accepted: May 12, 2023
Published: May 26, 2023

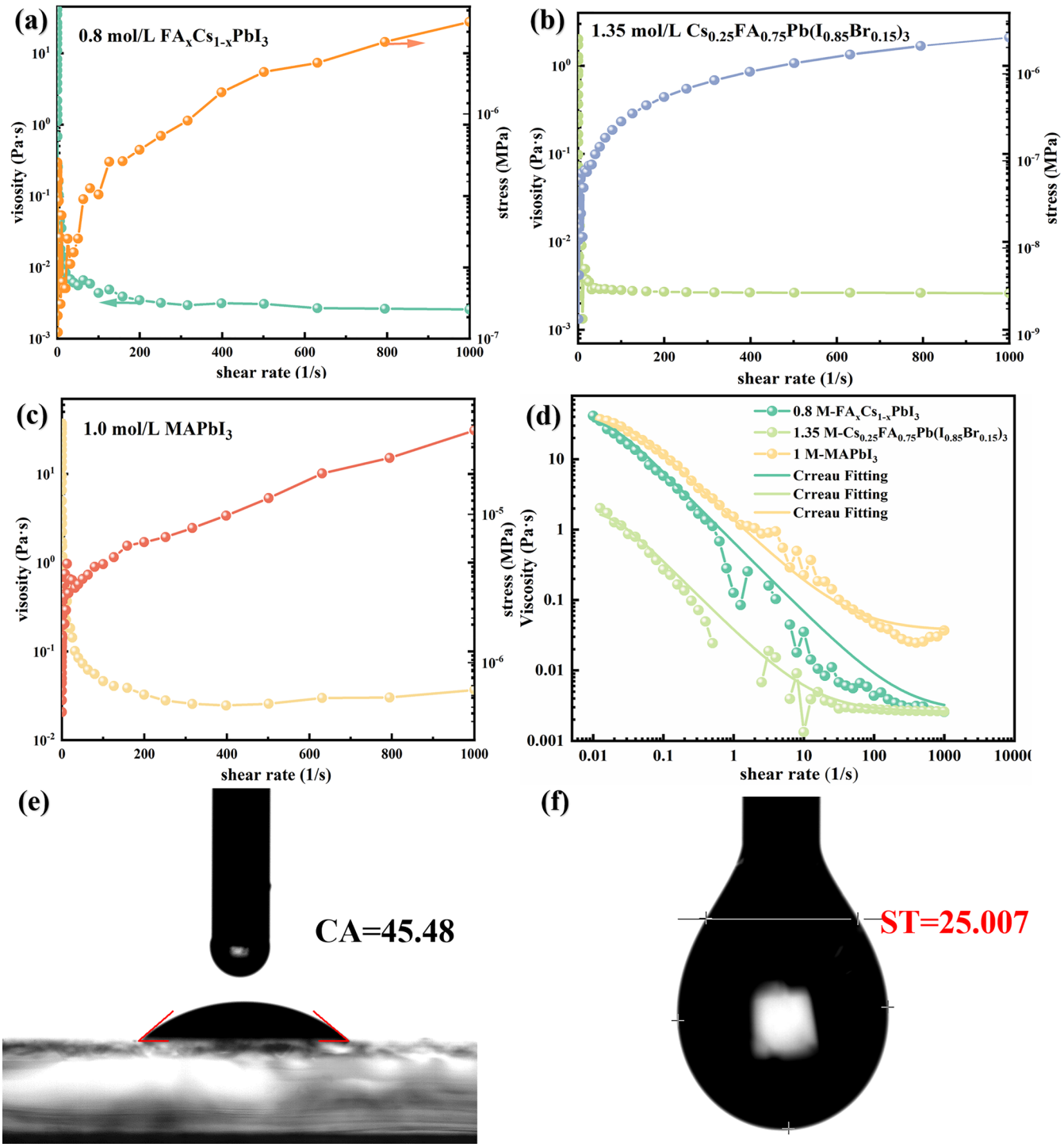

Figure 1. Rheological curves for (a) 0.8 M-$FA_xCs_{1-x}PbI_3$, (b) 1.35 M-$Cs_{0.25}FA_{0.75}Pb(I_{0.85}Br_{0.15})_3$, and (c) 1 M-$MAPbI_3$; (d) fitting results of rheological data of the solution; (e) dynamic contact angle between solution and substrate; and (f) surface tension.

large-area PSCs, aiming to promote the commercialization of slot-die coating applied to PSCs. However, the existing simulation works are mostly organized based on the Newtonian fluid or high-viscosity non-Newtonian fluid[21] but not low-viscosity non-Newtonian fluid (e.g., perovskite precursor solution). Thus, these works can sparingly provide guidance for preparing perovskite film. The previous studies mainly focused on the process of the fluid being coated on the substrate and tend to ignore the solution process flowing through the slit.[22,23] Nevertheless, this is a key procedure to enable the fluid to be uniformly extruded and coated on the substrate forming stable and continuous large-area wet film. In addition, the thickness of the solid film for high-performance PSCs is 0.5−1 μm. Correspondingly, the wet film ranges from 5 to 15 μm, which is far less than the film thickness in other application scenarios (e.g., the electrode of power lithium-ion cells is about 400 μm).[24] This issue indicates that the coating process for the perovskite film is quite different from other industries. Therefore, it is crucial to simulate the effects of key

https://doi.org/10.1021/acsomega.3c00959
ACS Omega 2023, 8, 19547−19555

parameters on preparing the stable and continuous perovskite wet film by slot-die coating.

In this work, the influence of process parameters such as liquid supply velocity (V_{in}), coating velocity (V), coating gap (H), and shim thickness (d) on the morphology of the wet film is investigated. First, this work analyzes the rheological characteristics of the typical perovskite precursor. Afterward, depending on the numerical methodology using Fluent, this work clarifies the film-forming process that the perovskite solution 0.8 M-$FA_xCs_{1-x}PbI_3$ passes through the slit (defined as the internal flow field) to be coated on the substrate (defined as the external flow field). Herein, different V_{in} and V are set to study the coupling relationship in key coating parameters and the corresponding effects on wet film. Finally, in this work, the process parameters controlling the preparation of a certain thickness range of homogeneous continuous perovskite wet film are obtained. Meanwhile, the minimum thickness of wet film that can be achieved under different coupling relationships is theoretically evaluated. Here, the reliability of this modeling work is verified by the laboratory experiments, and the results hopefully provide important guidance for the development and optimization during the slot-die coating process of the perovskite precursor approximating Newtonian fluid.

2. SIMULATION AND MODELING

2.1. Setting Parameters and Carreau Fitting. Previous studies have shown that three different perovskite precursors, that is, 0.8 M-$FA_xCs_{1-x}PbI_3$, 1.35 M-$Cs_{0.25}FA_{0.75}Pb(I_{0.85}Br_{0.15})_3$, and 1 M-$MAPbI_3$, prepared by slot-die coating can obtain high-efficiency and stable PSCs.[25−27] An advanced rotational rheometer (TA/DHR-2) is used to test the kinetic viscosity of these three solutions separately, where the shear rate scan range is 0.01−1000 r/s. The rheological curves of these solutions at room temperature are obtained, which indicate viscosity and shear stress as a function of shear rate, as shown in Figure 1a−c. It can be seen that all the perovskite solutions show the characteristics of shear thinning to be judged as pseudoplastic fluids. The Carreau model[28] (Formula 1) is used to fit the viscosity curves to clearly describe the fluid properties in the pseudoplastic zone as far as possible

$$\eta = \eta_\infty + (\eta_0 - \eta_\infty)/[1 + (\lambda\gamma)^a]^{1-n/a} \quad (1)$$

where η is the shear viscosity, η_∞ is the infinite shear viscosity, η_0 is the zero shear viscosity, λ is the relaxation time, γ is the shear rate, n is the non-Newtonian index, and a is the Yasuda index ($a = 2$). The fitting results are shown in Figure 1d, demonstrating that all the perovskite solutions belong to the low-viscosity fluid. Therefore, the 0.8 M-$FA_xCs_{1-x}PbI_3$ perovskite precursor dissolved in common solvent combination of *N*,*N*-dimethylformamide and *N*-methyl-2-pyrrolidone is taken as the follow-up research object in this work. The density (ρ) of 0.8 M-$FA_xCs_{1-x}PbI_3$ is 1486 kg/m^3 through the test. Figure 1e,f shows that the dynamic contact angle (θ_1) is 45.48° and the surface tension (σ) is 25.007 mN/m between 0.8 M-$FA_xCs_{1-x}PbI_3$ and the substrate, respectively. According to the actual experiment in previous achievements, the coating gap (H) and the size of slit (d) are determined as 80[29−31] and 50 μm, respectively.[13] The detailed setting parameters and Carreau fitting results (η_0, η_∞, n, and λ) of 0.8 M-$FA_xCs_{1-x}PbI_3$ are listed in Table 1, which are used for subsequent calculations.

Table 1. Physical Properties and Coating Parameters of 0.8 M-$FA_xCs_{1-x}PbI_3$

parameter	symbol	unit	value
zero shear viscosity	η_0	Pa·s	41.233
infinite shear viscosity	η_∞	Pa·s	0.00257
dimensionless parameter	n		0.07
time parameter	λ	s	65.45
density	ρ	kg/m^3	1486
pressure outlet	P	Pa	101 325
coating gap	H	μm	80
surface tension	σ	mN/m	25.007
dynamic contact angle	θ_1	deg	45.48
size of slit	d	μm	50

2.2. Internal and External Field Model. In this work, the common "T" type coating die with a single slot circular section is introduced as a reference. Meanwhile, the numerical simulations of three-dimensional (3D) internal field and two-dimensional (2D) external field are achieved by Fluent. Figure 2a exhibits the 3D simplified model of the coating head. During the coating process, the perovskite solution flows through the channel, homogenizing chamber, and slit in turn and is finally evenly extruded from the lip. The flow state of the fluid in the mold is mainly affected by the size and shape of the homogenizing chamber and slit area. Therefore, the geometric modeling is carried out after appropriate simplification of this part (Figure 2b), which is gridded by the finite volume method (FVM), as shown in Figure 2c. In addition, considering the velocity of the fluid in the thickness direction, the slit part is divided into six layers of quadrilateral mesh by a sweeping method. Finally, the global mesh size is set to 0.1 mm, and the mesh quality is over 0.3.

The 2D external model is shown in Figure 2d, which is the initial state of calculation that the perovskite fills the slit (marked with red) but does not flow out. When calculation starts, perovskite begins to flow to the air domain with a stable velocity. The whole domain is mainly divided into quadrilateral grid with an average size of 10^{-5} m and a quality over 0.7, while the exit as well as the motion boundary line size is adjusted to 10^{-6} m to accurately obtain the flow state at each motion boundary, as shown in Figure 2e. In this work, the three laws of mass, momentum, and energy conservation apply to the process of fluid flow. Although heat conduction exists during the fluid flow, it has sparing effect on the calculation results.[32] Therefore, to simplify the calculation, it is assumed that the system is isothermal, that is, no heat transfer or exchange occurs,[33] by which only the mass conservation continuity equation and the momentum conservation equation are used as the basic differential equations in the fluid simulation.[19,34] Furthermore, when the coating gap (H) is a constant, the influence of different liquid supply velocity (V_{in}) and coating velocity (V) on the velocity uniformity and wet film at the slit outlet is investigated. In the internal field, the screw pump controls a constant liquid supply velocity to inject perovskite precursor solution and thus it is regarded as a steady flow. The external field is considered as transient process due to changing contact between the coating bead and substrate. Besides, the dynamic contact angle between the solution and the substrate is 45°, and the static contact angle between the solution and the touch wall of the die is 160°. In order to ensure the convergence, the method is pressure implicit with splitting of operators and the time step is 10^{-4}.

https://doi.org/10.1021/acsomega.3c00959
ACS Omega 2023, 8, 19547−19555

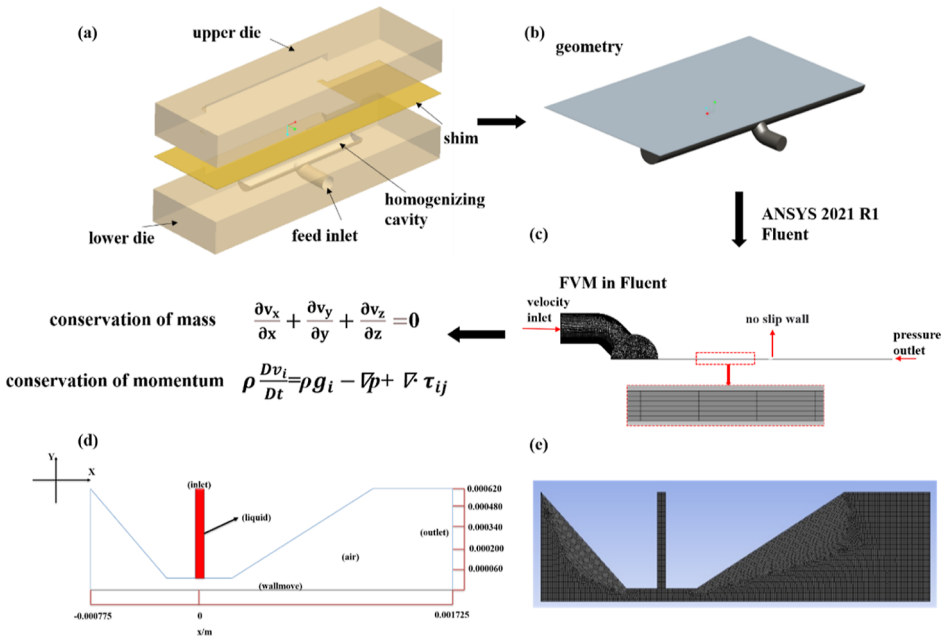

Figure 2. (a) Simplified model structure of coating die head; (b) geometry of internal field; (c) meshing of internal field based on FVM; (d) external field and boundary conditions; and (e) meshing of external field based on FVM.

3. RESULTS AND DISCUSSION

3.1. Simulation for Internal Flow Field. In the internal flow field, the 0.8 M-$FA_xCs_{1-x}PbI_3$ perovskite solution flows through the "T"-type die head with a slit of 50 μm. Different liquid supply velocities (V_{in}) are calculated to find the minimum V_{in} that can make the solution at the slit outlet extrude uniformly, thus facilitating uniform coating. In order to intuitively analyze the coating uniformity of solution at the slit outlet, the velocity distribution of the slurry at the center line of the slit outlet is quantitatively analyzed. Besides, the evaluation index of uniformity (U_v) is introduced[35]

$$U_v = 1 - 1/n\left(\sum_{i=1}^{n} |v_i - v_{ave}|/v_{ave}\right) \quad (2)$$

where U_v represents the velocity uniformity, v_i represents the velocity of layer i in the X-axis direction of the slit outlet, v_{ave} represents the average velocity, and 1 is an ideal uniform flow. U_v represents the difference between the weighted average of the percentage difference of velocity distribution at both ends of the outlet and the center and the ideal uniform flow. The greater the U_v is, the more uniform the velocity distribution becomes. The outlet velocity uniformity parameters corresponding to different V_{in} calculated by Formula 2 are listed in Table 2. When V_{in} is 0.0005 m/s, U_v is only 64.8%; comparatively, when V_{in} is increased to 0.0008 m/s, U_v reaches up to 99.6%. This phenomenon is mainly due to V_{in} which is too low and thus the solution wall surface adhesion causes uneven distribution in the die head, resulting in an uneven flow velocity from the slit outlet. Therefore, the V_{in} of 0.0008 m/s is considered as the minimum V_{in} of the system model.

Figure 3a,b is the pressure contour and velocity streamlines of die head when V_{in} is 0.0008 m/s, respectively. It can be observed that no vortex occurs in the whole flow field, and the pressure is evenly distributed transversely from the inlet to the outlet. The cross sections parallel to the YZ plane in the post-processing are used to facilitate the observation of velocity distribution in the homogenizing chamber, as shown in Figure 3c. After entering the homogenizing chamber from the inlet, the solution gradually disperses to both ends of cavity and the velocity decreases until to zero. Then, it flows out from the homogenizing chamber through the slit for secondary dispersion and homogenization. It can be seen from Figure 3d that the solution maintains a high shear rate and uniform distribution in the slit, and thus the solution keeps high uniformity of velocity when it flows to the slit outlet. In order to further analyze the velocity distribution at the slit outlet, a slit outlet centerline parallel to the X-axis is constructed, as shown in Figure 3e. When V_{in} is 0.0008 m/s, a symmetrical parabola is formed along the transverse direction of the solution flow velocity and the distribution is uniform, which proves the applicability of the geometric model about internal flow field for low-viscosity solution.

V_{in} of 0.0008 m/s corresponds to 99.6% of the high U_v; while V_{in} dropped to 0.0005 m/s, U_v is significantly lower than 0.0008 m/s, which is consistent with the calculation result of Formula 2 exhibiting in Figure 3f. In addition, Figure 4a shows

Table 2. Parameters of Different V_{in} and V_{out} Based on 50 μm "T" Type Model

V_{in} (m/s)	average of fluid (m/s)	V_{out} (m/s)	U_v (%)
0.0005	0.00024	0.00098	64.8
0.0008	0.00038	0.00157	99.6
0.0010	0.00048	0.00196	99.5
0.0050	0.00239	0.00981	91.9
0.0100	0.00479	0.01961	99.6
0.0150	0.00719	0.02942	99.6
0.0200	0.00958	0.03923	91.9
0.0500	0.02399	0.09807	99.6
0.1000	0.04813	0.19614	99.6
0.2000	0.09680	0.39228	99.6
0.5000	0.24409	0.98071	96.5
0.6000	0.28621	1.14036	99.6

https://doi.org/10.1021/acsomega.3c00959
ACS Omega 2023, 8, 19547−19555

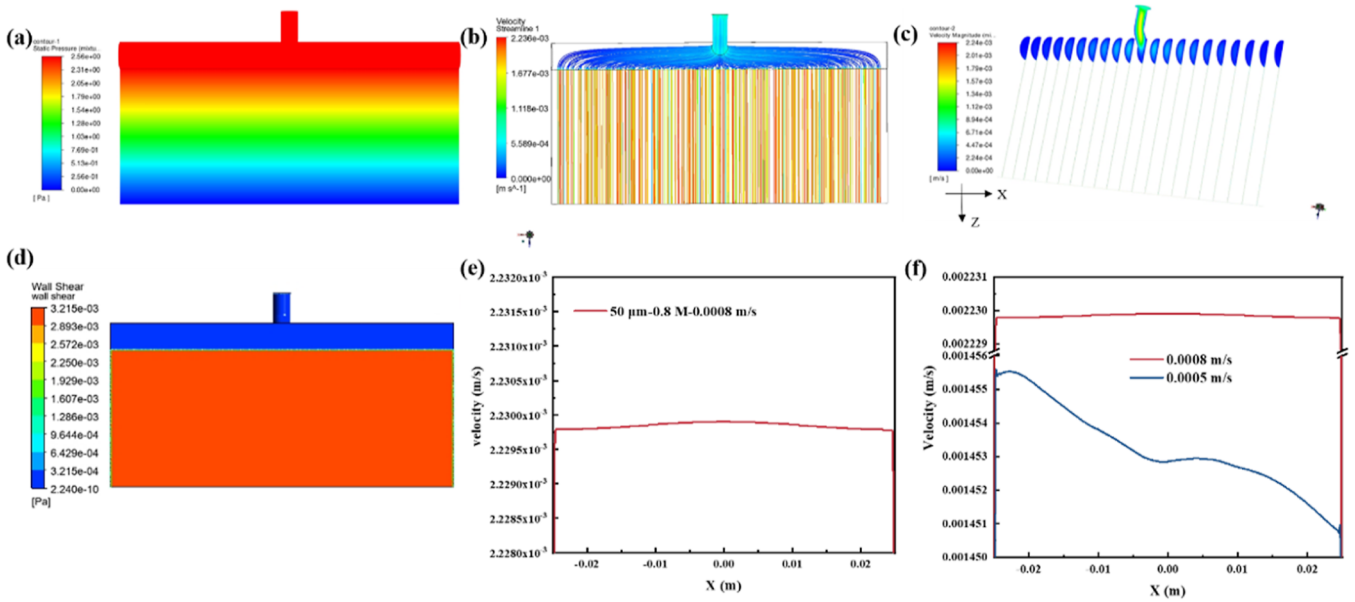

Figure 3. Simulation results of 0.8 M-perovskite solution flowing through a "T" cutter head with a slit size of 50 μm for (a) pressure contour; (b) velocity streamlines; (c) cross-sectional velocity distribution nephogram; (d) wall shear rate distribution nephogram; (e) velocity distribution curve of slit outlet center line when V_{in} is 0.0008 m/s; and (f) velocity distribution curves of slit outlet center line with V_{in} of 0.0008 and 0.0005 m/s.

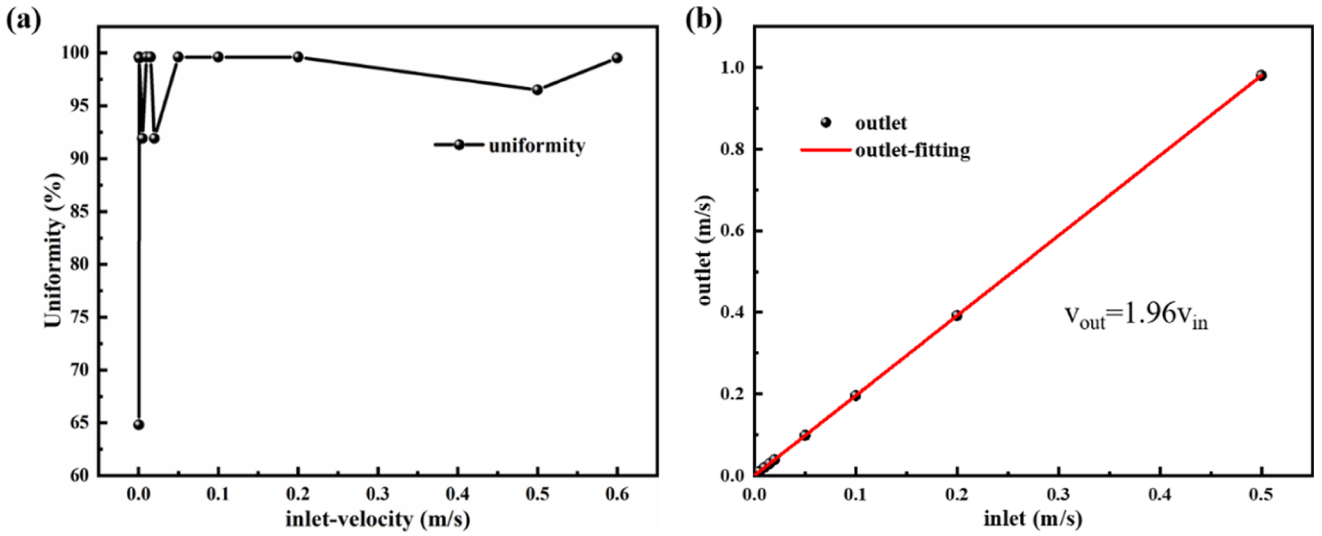

Figure 4. (a) Line graph of U_v corresponding to different V_{in} and (b) fitting results for V_{out} corresponding to different V_{in}.

the U_v curve with different V_{in}. It can be found that U_v maintains at a high level when V_{in} is higher than 0.0008 m/s to ensure the uniform extrusion of solution at the slit outlet, which is conducive to the uniform coating of solution on the substrate. According to the changes of parameters in Table 2, the relationship between the slit outlet velocity (V_{out}) and V_{in} can be obtained by linear fitting as $V_{out} = 1.96V_{in}$, as shown in Figure 4b, and it can be observed that there is a linear growth.

3.2. Simulation for External Flow Field. Results of the solution coating are determined by the stability of the coating bead during the process that the solution is extruded from the die and coated onto the moving substrate in the external flow field.[36,37] The influencing factors mainly include four main forces:

i. The viscous force that pulls the coated bead onto the moving substrate, $F_v = \mu V/H$;
ii. The inertial force of the fluid extruding from the die, which contributes to flow stability to a certain extent, and too much will cause the coated beads to lose stability, denoted as $F_i = \rho V_{in}^2$;
iii. The fluid surface tension F_σ;
iv. The gravitational force $F_{gv} = \rho gH$.

Figure 5 shows the fluid force analysis of the fluid obtained by analyzing the fluid flow in the coating process. In particular, Reynolds number is the ratio of inertial force to viscous force and when the Reynolds number is less than 1, the fluid flow is a laminar process.[38] According to the calculation, in the numerical model for preparing a perovskite film by slot-die coating, the inertial force formed by the solution impacting the moving substrate is less than the viscous force, that is, $Re < 1$. Therefore, the coating process in the external flow field is mainly dominated by F_v and the liquid flow is stable, which is regarded as laminar flow process.

https://doi.org/10.1021/acsomega.3c00959
ACS Omega 2023, 8, 19547−19555

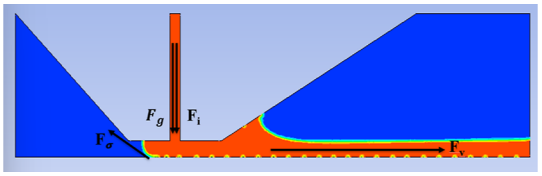

Figure 5. Fluid force analysis (viscous force F_v; gravitational force F_g; surface tension F_σ; and inertial force F_i).

V_{in} corresponding to the higher U_v obtained in the internal flow field simulation is the reference value for V_{in} in the external flow field calculation. Furthermore, different coating parameters are selected to simulate the morphology of wet film formed in a specific range when the coating gap (H) is 80 μm. As shown in Figure 6a–c, the coating process is sparingly affected by gravity. After the beginning of coating 0.025 s, the solution moves along the positive direction of X-axis (to the right) with the substrate due to the viscous force. However, the fluid is influenced by the surface tension and tends to disturb the wet film and make it unstable in the initial stage. As the coating proceeds, the upstream meniscus quickly reaches a stable state and the flow field is stabilized at 0.275 s. Figure 6e displays the volume fraction distribution of solution along the Y-axis at the outlet of the calculation domain. Accordingly, the thickness (h) of the wet film after coating stabilization under this process could be calculated as 10 μm.

Theoretically, when the liquid supply velocity is lower and the coating velocity is higher, a uniform and stable film can be obtained;[22] furthermore, as shown in Figure 6, it can be achieved when V_{in} is 0.01 m/s, as long as V is slightly higher than V_{in}. However, as V gradually increases based on Figure 6, uneven wet film thickness or porosity defects will occur. The phenomenon is due to excessive V and insufficient V_{in}. When V increases to 0.023 m/s, film breaking will occur as shown in Figure 7. On the contrary, when V is further reduced to 0.008 m/s, the wet film will be too thick to reach a stable state, as shown in Figure 8. It is mainly attributed that V is lower than the limit value and the V_{in} is too high, resulting that the solution accumulates on the substrate.

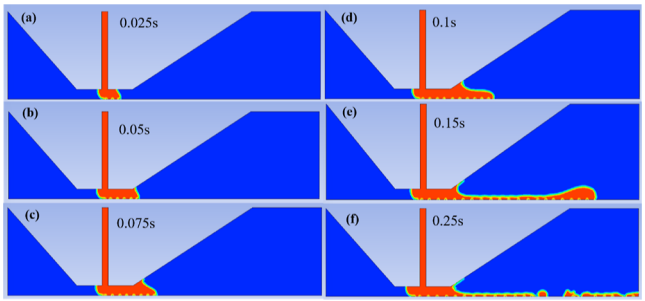

Figure 7. Wet film states at (a) 0.025, (b) 0.05, (c) 0.075, (d) 0.1, (e) 0.15, and (f) 0.25 s with the coating gap of 80 μm, a V_{in} of 0.01 m/s, and a V of 0.023 m/s.

The optional coating windows are the main index to evaluate the pre-measured slot-die coating method, which is usually characterized by capillary number (Ca). Ca represents the ratio of the viscous force generated by the substrate moving

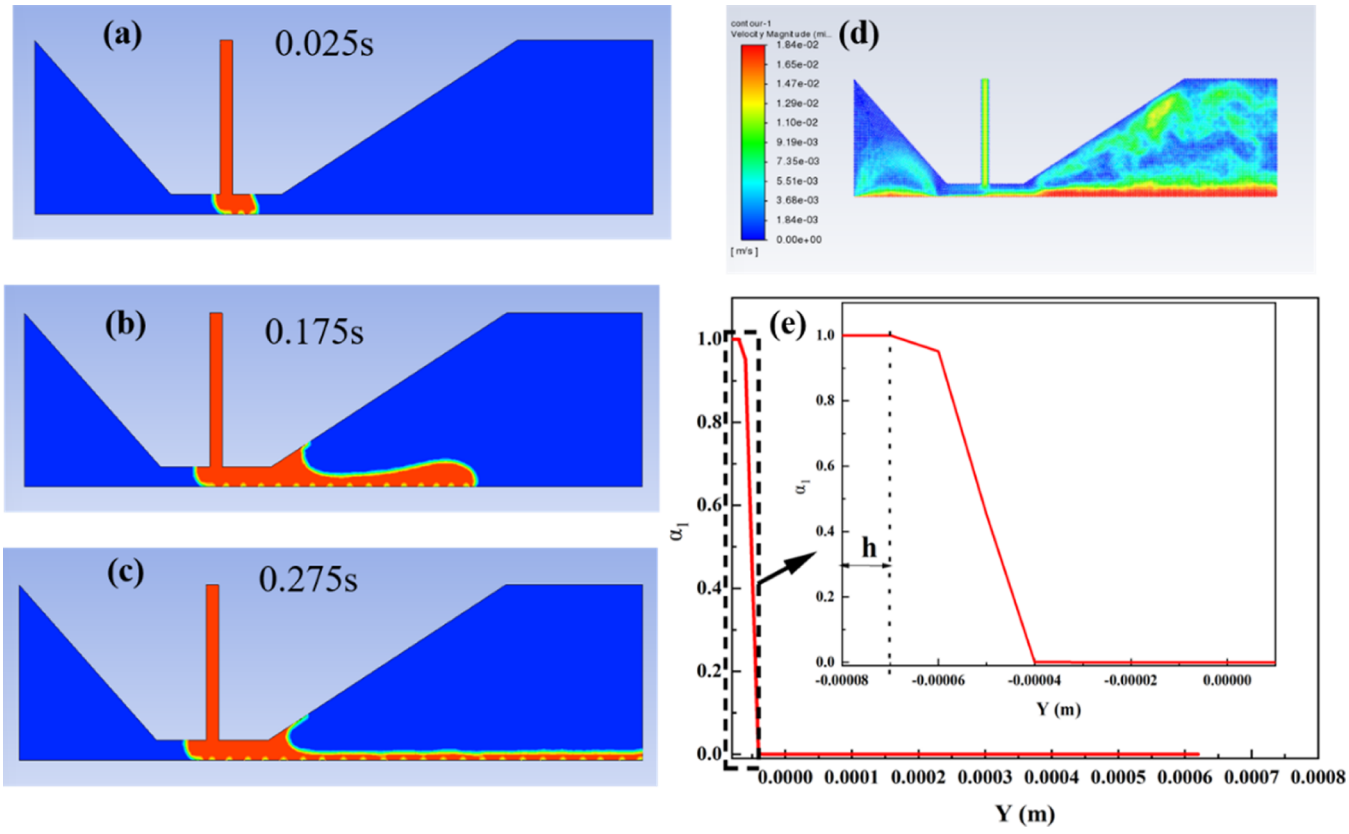

Figure 6. Coating gap of 80 μm, V_{in} of 0.01 m/s, V of 0.018 m/s, the wet film states at (a) 0.025, (b) 0.175, and (c) 0.275 s; (d) velocity distribution of flow field after coating stabilization; (e) calculation of the volume fraction of the solution at the exit of the domain (the inset is a partial enlargement).

https://doi.org/10.1021/acsomega.3c00959
ACS Omega 2023, 8, 19547−19555

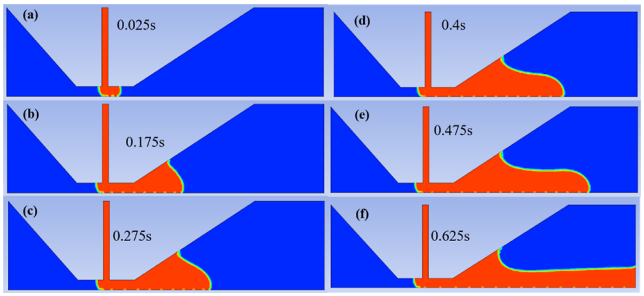

Figure 8. Wet film states at (a) 0.025, (b) 0.175, (c) 0.275, (d) 0.4, (e) 0.475, and (f) 0.625 s with the coating gap of 80 μm, a V_{in} of 0.01 m/s, and a V of 0.008 m/s.

in the fluid to the surface tension of the fluid, denoted as $Ca = \mu U/\sigma$. As shown in Figure 9a, when coating gap (H) and V_{in} are determined, h decreases with the increase of V. Moreover, for a certain value of Ca, when the thickness of wet film is less than the minimum value (h_{min}), a uniform film could not be formed. When V_{in} is 0.0050, 0.0100, 0.0150, 0.0500, and 0.1000 m/s, h_{min} is 20, 10, 10, 20, and 40 μm, which are basically in accordance with the equation $h_{min} = 0.67HCa^{2/3}$. Thus, when the properties of solution and the coating gap are constant, Ca must meet specific conditions to form selective coating windows to obtain uniform wet film.

Based on the calculation results of the internal flow field, the external field coating gap (H) is set to 80 μm. V_{in} is selected as 0.001, 0.005, 0.010, 0.015, 0.050, and 0.100 m/s, and the range of V is set as 0.002−0.150 m/s. A total of 38 groups of simulation experiments are designed within the selected range, and the results are shown in Figure 9b. Therein, the region B represents the area where V is too slow, which will lead to excessively thick wet film. The region C refers to the area where air enters the wet film and causes porosity defects. When V_{in} decreases again or the V increases, the film will be uneven or even broken as in region D. Besides, the region A refers to the parameter area where a uniform and stable wet film can be obtained, which is optional coating windows. For the upper boundary range of region A, the maximum value of V and V_{in} follows the fitting linear relationship of $V = 0.003 + 1.46V_{in}$ ($V_{in} \leq 0.1$ m/s), while for the lower boundary range of region A, the minimum value of V and V_{in} yields $V = 0.002 + 0.67V_{in}$ ($V_{in} \leq 0.1$ m/s). The right boundary of region A indicates that when the maximum V_{in} exceeds 0.1 m/s, the phenomenon of region D will be formed due to the excessive corresponding V. In addition, higher V corresponds to a larger range of selectable V_{in} in region A. Therefore, in the actual coating experiment, the expected uniform and stable wet film can be achieved only when the process parameters are selected within the A interval. Conversely, parameters beyond this range probably lead to defects.

4. RELIABILITY ANALYSIS

Referring to a numerical work, its reliability is of significance for the scientific recognition herein. Accordingly, three series of laboratory experiments were conducted, where three points (P1, P2, and P3) in the coating windows shown in Figure 9b were adopted for the model validation. Accordingly, the experimental outputs are exhibited in Figure 10, in which the

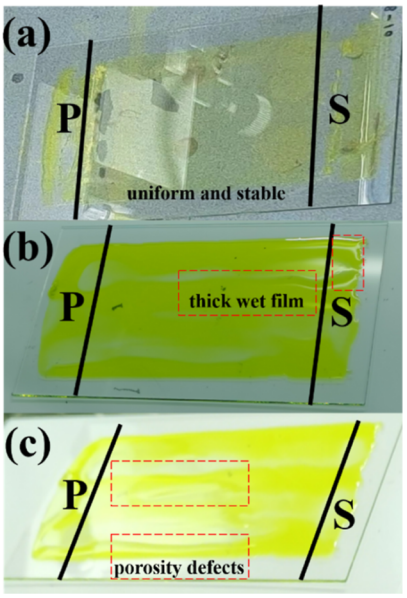

Figure 10. Wet film in different states obtained from laboratory experiments, (a) uniform and stable wet film; (b) thick wet film; and (c) porosity defects. S and P represent the start and end points of coating, respectively.

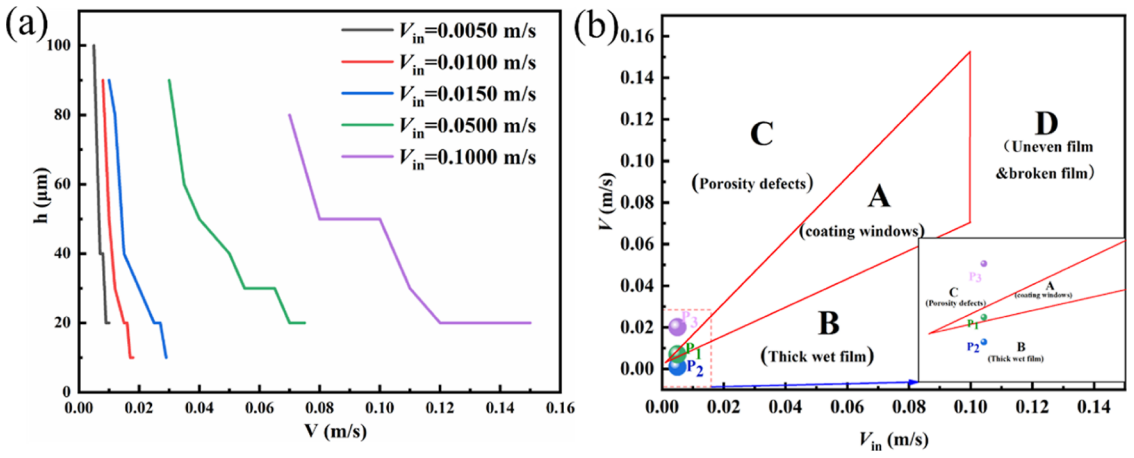

Figure 9. Coating gap of 80 μm (a) variation curves of wet film thickness h with coating velocity for different liquid supply velocities; (b) schematic diagram of coating windows and defect generation, including coating windows region A, thick wet film region B, porosity defects region C, and uneven film or broken film region D.

https://doi.org/10.1021/acsomega.3c00959
ACS Omega 2023, 8, 19547−19555

H, d and V_{in} are set as 80 μm, 50 μm, and 0.005 m/s, respectively. For all laboratory experiments, the coating starts from S and stops at P. Herein, the settings at P1 (V = 0.008 m/s) enables a uniform and stable wet film to be obtained (Figure 10a), while those at P2 (V = 0.001 m/s) and P3 (V = 0.02 m/s) induce the thick wet film and porosity defects, respectively (Figure 10b,c). That is to say, the situation as P1 ensures a better film output, compared to the experimental conditions at P2 and P3, which exhibits a similar recognition of the numerical model shown in Figure 9b. Basically, these experimental results correspond to the numerical simulations in a good manner, indicating that this modeling work is reliable.

5. CONCLUSIONS

This work adopts the finite element analysis method, using ANSYS Fluent software. Herein, a numerical model of the internal and external flow fields is constructed, which is suitable for the analysis of low-viscosity perovskite precursor solution with approximate Newtonian fluid characteristics. This model provides reliable basis for setting process parameters in slot-die coating. Accordingly, the following points are made:

For the preparation of 0.8 M-$FA_xCs_{1-x}PbI_3$, by simulating the effects of different liquid supply velocities (V_{in}) on slit outlet velocity (V_{out}) in the internal flow field, in which there is a linear correlation between them of $V_{out} = 1.96V_{in}$. The visual curves for the thickness of wet film with different coating velocities (V) was obtained, and different thicknesses of wet film can be realized by adjusting d and V_{in}.

When the minimum V_{in} is 0.0008 m/s, the uniformity of V_{out} can reach 99.6%; in addition, the coating windows for preparing uniform and continuous perovskite wet film with certain thickness by slot-die coating is achieved.

For the upper boundary range of the coating windows, the relationship of V and V_{in} is described as $V = 0.003 + 1.46V_{in}$ ($V_{in} \leq 0.1$ m/s), while for the lower boundary range, the value of V and V_{in} meets $V = 0.002 + 0.67V_{in}$ ($V_{in} \leq 0.1$ m/s); when V_{in} is higher than 0.1 m/s, film will break due to the excessive V.

AUTHOR INFORMATION

Corresponding Author

Xia Hao − *Institute of New Energy and Low-Carbon Technology & College of Materials Science and Engineering, Sichuan University, Chengdu 610064, P. R. China; Engineering Research Center of Alternative Energy Materials & Devices, Ministry of Education, Chengdu 610065, P. R. China;* orcid.org/0000-0002-3512-9600; Email: hao.xia0808@scu.edu.cn

Authors

Qiang Guo − *Institute of New Energy and Low-Carbon Technology & College of Materials Science and Engineering, Sichuan University, Chengdu 610064, P. R. China*

Xiaoli Gong − *Institute of New Energy and Low-Carbon Technology & College of Materials Science and Engineering, Sichuan University, Chengdu 610064, P. R. China*

Zhenzhen Shen − *Institute of New Energy and Low-Carbon Technology & College of Materials Science and Engineering, Sichuan University, Chengdu 610064, P. R. China*

Jingquan Zhang − *Institute of New Energy and Low-Carbon Technology & College of Materials Science and Engineering, Sichuan University, Chengdu 610064, P. R. China; Engineering Research Center of Alternative Energy Materials & Devices, Ministry of Education, Chengdu 610065, P. R. China;* orcid.org/0000-0002-5346-2730

Complete contact information is available at: https://pubs.acs.org/10.1021/acsomega.3c00959

Notes

The authors declare no competing financial interest.

ACKNOWLEDGMENTS

This work was supported by the National Key Research and Development Program of China (no. 2019YFE0120000); the Science and Technology Program of Sichuan Province (nos. 2022NSFSC0268, 2022YFG0296; 2021YFG0102, 2020YFH0079, 2019YFG0513, and 2019ZDZX0015); Engineering Featured Team Fund of Sichuan University (no. 2020SCUNG102); and Creative Project of Engineering Research Center of Alternative Energy Materials & Devices, Ministry of Education, Sichuan University (grant no. AEMD-C202201).

REFERENCES

(1) Kojima, A.; Teshima, K.; Shirai, Y.; Miyasaka, T. Organometal Halide Perovskites as Visible-Light Sensitizers for Photovoltaic Cells. *J. Am. Chem. Soc.* **2009**, *131*, 6050−6051.

(2) Lee, M. M.; Teuscher, J.; Miyasaka, T.; Murakami, T. N.; Snaith, H. J. Efficient Hybrid Solar Cells Based on Meso-Superstructured Organometal Halide Perovskites. *Science* **2012**, *338*, 643−647.

(3) Kosyachenko, L. A.; Mathew, X.; Roshko, V. Y.; Grushko, E. V. Optical absorptivity and recombination losses: The limitations imposed by the thickness of absorber layer in CdS/CdTe solar cells. *Sol. Energy Mater. Sol. Cells* **2013**, *114*, 179−185.

(4) Park, J.; Kim, J.; Yun, H. S.; Paik, M. J.; Noh, E.; Mun, H. J.; Kim, M. G.; Shin, T. J.; Seok, S. I. Controlled growth of perovskite layers with volatile alkylammonium chlorides. *Nature* **2023**, *616*, 724−730.

(5) Min, H.; Lee, D. Y.; Kim, J.; Kim, G.; Lee, K. S.; Kim, J.; Paik, M. J.; Kim, Y. K.; Kim, K. S.; Kim, M. G.; et al. Perovskite solar cells with atomically coherent interlayers on SnO(2) electrodes. *Nature* **2021**, *598*, 444−450.

(6) Liang, Q.; Liu, K.; Sun, M.; Ren, Z.; Fong, P. W. K.; Huang, J.; Qin, M.; Wu, Z.; Shen, D.; Lee, C. S.; et al. Manipulating Crystallization Kinetics in High-Performance Blade-Coated Perovskite Solar Cells via Cosolvent-Assisted Phase Transition. *Adv. Mater.* **2022**, *34*, No. e2200276.

(7) Li, H.; Zhou, J.; Tan, L.; Li, M.; Jiang, C.; Wang, S.; Zhao, X.; Liu, Y.; Zhang, Y.; Ye, Y.; et al. Sequential vacuum-evaporated perovskite solar cells with more than 24% efficiency. *Sci. Adv.* **2022**, *8*, No. eabo7422.

(8) Du, M.; Zhao, S.; Duan, L.; Cao, Y.; Wang, H.; Sun, Y.; Wang, L.; Zhu, X.; Feng, J.; Liu, L.; et al. Surface redox engineering of vacuum-deposited NiOx for top-performance perovskite solar cells and modules. *Joule* **2022**, *6*, 1931−1943.

(9) Gil-Escrig, L.; Dreessen, C.; Palazon, F.; Hawash, Z.; Moons, E.; Albrecht, S.; Sessolo, M.; Bolink, H. J. Efficient Wide-Bandgap Mixed-Cation and Mixed-Halide Perovskite Solar Cells by Vacuum Deposition. *ACS Energy Lett.* **2021**, *6*, 827−836.

(10) Cao, X.; Zhi, L.; Jia, Y.; Li, Y.; Zhao, K.; Cui, X.; Ci, L.; Zhuang, D.; Wei, J. A Review of the Role of Solvents in Formation of High-Quality Solution-Processed Perovskite Films. *ACS Appl. Mater. Interfaces* **2019**, *11*, 7639−7654.

(11) Le, T. S.; Saranin, D.; Gostishchev, P.; Ermanova, I.; Komaricheva, T.; Luchnikov, L.; Muratov, D.; Uvarov, A.; Vyacheslavova, E.; Mukhin, I.; et al. All-Slot-Die-Coated Inverted

Perovskite Solar Cells in Ambient Conditions with Chlorine Additives. *Sol. RRL* **2021**, *6*, 2100807.
(12) Yang, J.; Lim, E. L.; Tan, L.; Wei, Z. Ink Engineering in Blade-Coating Large-Area Perovskite Solar Cells. *Adv. Energy Mater.* **2022**, *12*, 2200975.
(13) Xu, K.; Al-Ashouri, A.; Peng, Z. W.; Kohnen, E.; Hempel, H.; Akhundova, F.; Marquez, J. A.; Tockhorn, P.; Shargaieva, O.; Ruske, F.; et al. Slot-Die Coated Triple-Halide Perovskites for Efficient and Scalable Perovskite/Silicon Tandem Solar Cells. *ACS Energy Lett.* **2022**, *7*, 3600−3611.
(14) Huang, S. H.; Guan, C. K.; Lee, P. H.; Huang, H. C.; Li, C. F.; Huang, Y. C.; Su, W. F. Toward All Slot-Die Fabricated High Efficiency Large Area Perovskite Solar Cell Using Rapid Near Infrared Heating in Ambient Air. *Adv. Energy Mater.* **2020**, *10*, 2001567.
(15) Du, M.; Zhu, X.; Wang, L.; Wang, H.; Feng, J.; Jiang, X.; Cao, Y.; Sun, Y.; Duan, L.; Jiao, Y.; et al. High-Pressure Nitrogen-Extraction and Effective Passivation to Attain Highest Large-Area Perovskite Solar Module Efficiency. *Adv. Mater.* **2020**, *32*, No. e2004979.
(16) Gong, C.; Fan, B.; Li, F.; Xing, Z.; Meng, X.; Hu, T.; Hu, X.; Chen, Y. An enhanced couette flow printing strategy to recover efficiency losses by area and substrate differences in perovskite solar cells. *Energy Environ. Sci.* **2022**, *15*, 4313−4322.
(17) Deng, Y.; Van Brackle, C. H.; Dai, X.; Zhao, J.; Chen, B.; Huang, J. Tailoring solvent coordination for high-speed, room-temperature blading of perovskite photovoltaic films. *Sci. Adv.* **2019**, *5*, No. eaax7537.
(18) Huang, T.; Tan, P.; Zhong, Z.; Li, M.; Zhang, Y.; Zhou, H. Numerical and experimental investigation on the defect formation in lithium-ion-battery electrode-slot coating. *Chem. Eng. Sci.* **2022**, *258*, 117744.
(19) Jang, I.; Song, S. A model for prediction of minimum coating thickness in high speed slot coating. *Int. J. Heat Fluid Flow* **2013**, *40*, 180−185.
(20) Park, J. S.; Yoo, T.; Chun, B.; Lee, K.-Y.; Jung, H. W. Operability limits for non-Newtonian liquids in dual-layer slot coating processes using the viscocapillary model. *J. Coat. Technol. Res.* **2021**, *19*, 35−47.
(21) Ding, X.; Liu, J.; Harris, T. A. L. A review of the operating limits in slot die coating processes. *AIChE J.* **2016**, *62*, 2508−2524.
(22) Goda, T.; Sasaki, Y.; Mizuno, M.; Morizawa, K.; Katakura, H.; Tomiya, S. Numerical analysis for predicting the operability window of slot-die coating onto porous media. *J. Coat. Technol. Res.* **2017**, *14*, 1053−1060.
(23) Wang, C.-C.; Zheng, Y.-Y. Numerical study of slot-die coating on film formation for different die lip configurations. *J. Chin. Inst. Eng.* **2021**, *44*, 637−645.
(24) Diehm, R.; Weinmann, H.; Kumberg, J.; Schmitt, M.; Fleischer, J.; Scharfer, P.; Schabel, W. Edge Formation in High-Speed Intermittent Slot-Die Coating of Disruptively Stacked Thick Battery Electrodes. *Energy Technol.* **2019**, *8*, 1900137.
(25) Bu, T.; Ono, L. K.; Li, J.; Su, J.; Tong, G.; Zhang, W.; Liu, Y.; Zhang, J.; Chang, J.; Kazaoui, S.; et al. Modulating crystal growth of formamidinium−caesium perovskites for over 200 cm2 photovoltaic sub-modules. *Nat. Energy* **2022**, *7*, 528−536.
(26) Dai, X.; Chen, S.; Jiao, H.; Zhao, L.; Wang, K.; Ni, Z.; Yu, Z.; Chen, B.; Gao, Y.; Huang, J. Efficient monolithic all-perovskite tandem solar modules with small cell-to-module derate. *Nat. Energy* **2022**, *7*, 923−931.
(27) Li, J.; Dagar, J.; Shargaieva, O.; Flatken, M. A.; Köbler, H.; Fenske, M.; Schultz, C.; Stegemann, B.; Just, J.; Többens, D. M.; et al. 20.8% Slot-Die Coated $MAPbI_3$ Perovskite Solar Cells by Optimal DMSO-Content and Age of 2-ME Based Precursor Inks. *Adv. Energy Mater.* **2021**, *11*, 2003460.
(28) Carreau, P. J. Rheological Equations from Molecular Network Theories. *Trans. Soc. Rheol.* **1972**, *16*, 99−127.
(29) Zimmermann, I.; Provost, M.; Mejaouri, S.; Al Atem, M.; Blaizot, A.; Duchatelet, A.; Collin, S.; Rousset, J. Industrially Compatible Fabrication Process of Perovskite-Based Mini-Modules Coupling Sequential Slot-Die Coating and Chemical Bath Deposition. *ACS Appl. Mater. Interfaces* **2022**, *14*, 11636−11644.
(30) Wu, Z.; Liu, X.; Zhong, H.; Wu, Z.; Chen, H.; Su, J.; Xu, Y.; Wang, X.; Li, X.; Lin, H. Natural Amino Acid Enables Scalable Fabrication of High-Performance Flexible Perovskite Solar Cells and Modules with Areas over 300 cm(2). *Small Methods* **2022**, *6*, No. e2200669.
(31) Yang, Z.; Zhang, W.; Wu, S.; Zhu, H.; Liu, Z.; Liu, Z.; Jiang, Z.; Chen, R.; Zhou, J.; Lu, Q.; et al. Slot-die coating large-area formamidinium-cesium perovskite film for efficient and stable parallel solar module. *Sci. Adv.* **2021**, *7*, No. eabg3749.
(32) Fuaad, P. A.; Swerin, A.; Lundell, F.; Toivakka, M. Simulation of slot-coating of nanocellulosic material subject to a wall-stress dependent slip-velocity at die-walls. *J. Coat. Technol. Res.* **2021**, *19*, 111−120.
(33) Park, J.; Kim, S.; Lee, C. An Analysis of Pinned Edge Layer of Slot-Die Coated Film in Roll-to-Roll Green Manufacturing System. *Int. J. Precis. Eng. Manuf.-Green Technol.* **2018**, *5*, 247−254.
(34) Lin, C.-F.; Hill Wong, D. S.; Liu, T.-J.; Wu, P.-Y. Operating windows of slot die coating: Comparison of theoretical predictions with experimental observations. *Adv. Polym. Technol.* **2010**, *29*, 31−44.
(35) Li, T.; Jin, S. P.; Huang, S.; Liu, W. Evaluation indices of flow velocity distribution uniformity: comparison and application. *Therm. Power Gener.* **2013**, *42*, 60−63+92.
(36) Chang, H.-M.; Chang, Y.-R.; Lin, C.-F.; Liu, T.-J. Comparison of vertical and horizontal slot die coatings. *Polym. Eng. Sci.* **2007**, *47*, 1927−1936.
(37) Romero, O. J.; Scriven, L. E.; Carvalho, M. S. Slot coating of mildly viscoelastic liquids. *J. Non-Newtonian Fluid Mech.* **2006**, *138*, 63−75.
(38) Chang, Y. R.; Chang, H. M.; Lin, C. F.; Liu, T. J.; Wu, P. Y. Three minimum wet thickness regions of slot die coating. *J. Colloid Interface Sci.* **2007**, *308*, 222−230.

https://doi.org/10.1021/acsomega.3c00959
ACS Omega 2023, 8, 19547−19555